Supporting Information for

Bifurcate Responses of Tidal Range to Sea-level Rise in Estuaries with Marsh Evolution

Xun Cai[1,2], Qubin Qin[1], Jian Shen[1], Yinglong J. Zhang[1]

[1]Virginia Institute of Marine Science, William & Mary, Gloucester Point, VA 23062, USA

[2]ORISE Research Participation Program at EPA, Chesapeake Bay Program Office, Annapolis, MD 21401, USA

The supporting information includes:

Section 1. Equations for tidal range and its change under SLR

Consider a tide propagating in a quasi-1D estuary with slowing varying cross-sectional area, with the origin located at the mouth and x-axis pointing into the direction of tidal propagation, the 1-D tidal energy equation according to Green's law can be described as (van Rijn, 2011):

$$\frac{d(EC_g b)}{dx} = -bS_D + bS \quad \text{(S1)}$$

where E is tidal energy per unit area, b is width, C_g is the group speed of the tide across the cross-section and it equals phase velocity C as a shallow water wave, S_D is the energy dissipation rate by bottom friction per unit width, S is the net energy input rate due to other physical forcings (e.g., baroclinic and barotropic forcings). Eq. (S1) only considers propagating tidal wave and omits the reflection and resonance of the tidal wave. The phase velocity $C = \sqrt{gh}$, where h is the laterally-averaged effective water depth, assuming the tidal range H << h (Friedrichs and Aubre, 1994). Thus, in Eq. (S1), $C_g b$ or Cb is related to the bathymetry of the estuary, and its impact on the change in tidal energy or range is the tidal shoaling effect: in a convergent estuary (i.e., h and/or b decrease with x), $\frac{d(C_g b)}{dx} > 0$, which tends to increase tidal energy.

Integrating Eq. (S1) over x gives:

$$ECb - E_0 C_0 b_0 = -\int_0^x (bS_D)dx \quad \text{(S2)}$$

where E_0, C_0 and b_0 are the tidal energy, phase velocity, and width at the mouth (x = 0), respectively. Rearranging Eq. (S2) gives:

$$E = \frac{E_0 C_0 b_0 - F}{Cb} = E_0 \left(\frac{C_0 b_0}{Cb}\right)\left(1 - \frac{F}{E_0 C_0 b_0}\right) \quad \text{(S3)}$$

where $F = \int_0^x (bS_D + bS)dx$ is the integration of the net cross-sectionally integrated energy dissipation from the mouth to the location x, and $\frac{F}{E_0 C_0 b_0}$ is the ratio of F to the energy flux at the mouth. Obviously, $E_0 C_0 b_0 > F$ must hold for a meaningful solution. According to the expression for tidal energy per unit horizontal area (E) and tidal range (H), $E = \frac{1}{8}\rho g H^2$, where ρ is water density and g = 9.8 m s^{-2} is the gravity, we get the expression for the tidal range H at any location x:

$$H = H_0 \sqrt{\frac{\rho_0}{\rho}} \sqrt{\frac{C_0 b_0}{Cb}} \sqrt{1 - \left(\frac{F}{E_0 C_0 b_0}\right)} \tag{S4}$$

where H_0 and ρ_0 are tidal range and water density at the mouth (x = 0). Setting the nondimensional parameters $\varepsilon_1 = \sqrt{1 - \left(\frac{F}{E_0 C_0 b_0}\right)}$ and $\varepsilon_2 = \sqrt{\frac{Cb}{C_0 b_0}}$, we can rewrite Eq. (S4) as

$$H = H_0 \frac{\varepsilon_1}{\varepsilon_2} \tag{S5}$$

Note that the spatial gradients in ρ is neglected. Thus, the tidal range at a location is determined by the net energy change by physical forcings, denoted by ε_1, and tidal shoaling effect, denoted by ε_2. $\varepsilon_1 < 1$ denotes that the physical forcings net increase the tidal energy, and $\varepsilon_1 > 1$ denotes that the physical forcings net decrease the tidal energy. $\varepsilon_2 < 1$ denotes that the estuary is convergent and the tidal shoaling effect increases the tidal energy, and $\varepsilon_2 > 1$ denotes that tidal shoaling effect decreases the tidal energy. In most shallow estuaries, bottom friction is a dominant forcing on tidal propagation (Talke and Jay, 2020); thus, on a long-term timescale, the net energy change F may be dominated by the energy dissipation by the bottom friction, which corresponds to a positive F and that $\varepsilon_1 < 1$. If the bottom frictional dissipation is less than the tidal energy convergence by the shoaling effect during the propagation (i.e., $\varepsilon_1 > \varepsilon_2$), the tidal range grows upstream; if the bottom frictional dissipation dominates the energy change (i.e., $\varepsilon_1 < \varepsilon_2$), the tidal range decays upstream. Eq. (S5) clearly show whether the tidal range increases or decreases over traveling distance is determined by the competition between shoaling effect and bottom frictional dissipation, which has been well known in previous studies using a variety of analytical solutions of shallow water equations (e.g., Jay, 1991; Friedrichs and Aubre, 1994; Prandle, 2003; Toffolon and Savenije, 2011; van Rijn, 2011).

After SLR, values of parameters change correspondingly. The ratio of the new tidal range to the original tidal range is:

$$\frac{H'}{H} = \frac{H_0{}'\frac{\varepsilon_1{}'}{\varepsilon_2{}'}}{H_0\frac{\varepsilon_1}{\varepsilon_2}} = \left(\frac{H_0{}'}{H_0}\right)\left(\frac{\varepsilon_1{}'}{\varepsilon_1}\right)/\left(\frac{\varepsilon_2{}'}{\varepsilon_2}\right) \tag{S6}$$

where the prime denotes the changed parameters after SLR, and $\varepsilon_1{}' = \sqrt{1 - \left(\frac{F'}{E_0{}'C_0{}'b_0{}'}\right)}$ and $\varepsilon_2{}' = \sqrt{\frac{C'b'}{C_0{}'b_0{}'}}$.

Set $\Delta Shoaling = \left(\frac{\varepsilon_2{}'}{\varepsilon_2}\right)$ to denote the impact of the change in shoaling effect on tidal range and $\Delta Friction = \left(\frac{\varepsilon_1{}'}{\varepsilon_1}\right)$ to denote the impact of the change in bottom frictional dissipation, Eq. (S6) becomes:

$$\frac{H'}{H} = \left(\frac{H_0{}'}{H_0}\right)\frac{\Delta Friction}{\Delta Shoaling} \tag{S7}$$

Thus, whether the tidal range increases or decreases under SLR is also determined by the competition between changes in shoaling effect and bottom frictional dissipation, besides the change in incoming tidal range at the mouth ($\frac{H_0{}'}{H_0}$).

For a system where the mouth is relatively deep compared with the SLR and the width at the mouth is relatively large compared with the change in width, the incoming tidal flux changes relatively small after SLR, leading to $\frac{H_0{}'}{H_0} \approx 1$. With water depth ($h$) or width (b) increases, $\Delta Shoaling > 1$, which tends to decrease tidal range. On the other hand, frictional dissipation also changes and determines $\Delta Friction$. If frictional dissipation decreases, which is generally the case in shallow areas, $\Delta Friction > 1$ and tends to increase tidal range.

Section 2. Study site and available data

The Pamunkey River and Mattaponi River are confluent at West Point upper stream of York River, which is one of the major tidal tributaries in lower Chesapeake Bay (Bay thereafter). The York-Pamunkey-Mattaponi Estuary is featured by convergent channels, well-developed shoals below the West Point, and a large extend of marsh adjacent to the nearly pristine Pamunkey River and Mattaponi river (Fig. S1c). The York River is about 50 km in length from the Goodwin Island to the West Point. The tidal portion of Pamunkey River extends about 90 km from the West Point, while the Mattaponi River has a tidal portion of about 70 km towards the fall line near Beulahville (Brooks, 1983; US Geological Survey, 2002, http://water.usgs.gov). The width of the York River varies from 4 km near its mouth to several hundreds of meters at the meanders in the Pamunkey River and Mattaponi river (Nichols and Kim, 1991). The channel depth of these three rivers varies. Along the York River, the channel depth tends to decrease from 20 m at the Gloucester Point to 6 m at the West Point (Fig. S1). The channel depth of the Pamunkey and the Mattaponi can reach 17 m and are commonly over 7 m in the lower portions (Fig. S1ab; Hobbs, 2009). The Pamunkey River has over 29.2 km^2 of tidal marshes and forested wetlands adjacent to the meanders, which occur to about 72 river kilometers from the West Point (Fig. S1c; Mitchell et al., 2017). On the Mattaponi, tidal marshes are found from its mouth to approximately 50 river kilometers, occurring in an area of 21.4 km^2 (Fig. S1c; Mitchell et al., 2017).

The York estuary is a microtidal estuary, whose mean tidal range increases from 0.7 m at the mouth to 0.85 m at the West Point according to the historical data (Fig. S4a; https://tidesandcurrents.noaa.gov/historic_tide_tables.html). Sweet Hall is considered to be a relatively low tidal range point along the Pamunkey River, where the historical tidal range is 0.75 m, and then the tidal range increases towards 1 m upwards. On the other side, the tidal range increases towards more than 1 m from the West Point in the Mattaponi River. For model validation, high-frequency measured elevation or depth date from both the NOAA tidal gauges of the main Bay (Fig. S1a) and the two VECOS stations along the Pamunkey River (Stations SH and WH) (Fig. S1b; VECOS, http://vecos.vims.edu) are used in this study. The historical tidal range from the NOAA tide tables and VECOS is also used for validation in this study (Fig. S1b). As the historical bathymetry of York may differ from current bathymetry, the tidal table data were used as a reference.

Section 3. Numerical Model

SCHISM (Semi-implicit Cross-scale Hydroscience Integrated System Model; www.schism.wiki) is employed in this study (Zhang et al., 2016; Ye et al., 2018). The model grid generally follows the one conducted in the Chesapeake Bay by Ye et al. (2018) and by Cai et al. (2020) with local refinements over the York-Pamunkey-Mattaponi Estuary. The grid covers the whole Bay towards the shelf break. The grid contains 47,316 nodes and 73,171 mixed triangular-quadrangular elements. The resolution varies from 2.4 km for the continental shelf to about 550 m in the Bay mouth (Fig. S2d), and less than 50 m in the marshes (Fig. S2a). From the York river to Pamunkey River and Mattaponi River, the along-channel resolution varies from 300 m outside the river month to 100 m in the upper stream, and the cross-channel resolution decreases from 200 m to less than 100 m (Fig. S2bc). The flexible vertical grid system LSC^2 (Localized Sigma Coordinates with Shaved Cells) has from 52 layers at deep regions to 2 layers at shallow regions. The average number of vertical layers in the whole domain is 12.7, which forms a total of 934,413 prisms. The topo-bathymetric information for the domain is mainly from the USGS Coastal National Elevation Database (CoNED; https://www.usgs.gov/land-resources/eros/coned), supplemented by the NOAA Chesapeake Bay (M130) Bathymetric Digital Model (https://data.noaa.gov/dataset/dataset/chesapeake-bay-m130-bathymetric-digital-elevation-model-noaa-nos-estuarine-bathymetry) and navigation charts (https://www.charts.noaa.gov/InteractiveCatalog/nrnc.shtml). In marsh areas initiated by the USGS topography map (https://www.usgs.gov/core-science-systems/ngp/tnm-delivery/topographic-maps) and Tidal Marsh Inventory (TMI; CCRM, VIMS; Mitchell et al., 2017), the drag induced by vegetation on flows are simulated with a semi-implicit time-stepping method implicitly (Zhang et al., 2020). The plant density is set to be 100 per m^2, the canopy height is assumed to be 1 m, and the drag coefficient is set to be 1.13 based on the value choice in Zhang et al. (2020).

The model simulation period is the year 2010 with a single non-split time step of 150 sec. The open boundary is forced by interpolated elevations from two tidal gauges at Lewes, DE, and Beaufort, NC. The temperature is nudged to the HYCOM for the simulated year. The salinity relaxation near the boundary utilized World Ocean Atlas monthly climatological data. Hydrologic loadings are from the outputs from Phase 6 Watershed Model of the Chesapeake Bay Assessment Tool (CAST) (Shenk and Linker, 2013). The North American Regional Reanalysis provides atmospheric forcing (Mesinger et al., 2006). The model was spun up for 1 year before simulating the period.

Section 4. Model assessment

The model is validated for both the main Bay area and the specific study area – York-Pamunkey-Mattaponi Estuary. In the main Bay, sub-tidal frequency signals at the NOAA gauges are compared to the modeled results (Fig. S1a). The simulated free-surface elevation agrees well with observation (not shown). The amplitudes and phases of the major constituents are captured according to the harmonic analysis (Fig. S3). The largest error for the M2 amplitude (2.26 cm) happens at station Tolchester in the upper Bay. The model tends to over-estimate the amplitudes in the Bay except at the station Swells, which is at the mouth of lower James River in the lower Bay.

In the York estuary, there are two VECOS stations providing high-frequency measurement of total water depth data, besides the historical tidal range from the NOAA tides tables, to validate the model (Fig. S1b). The mean modeled tidal range in 2010 along the York-Pamunkey-Mattaponi River transect is calculated as the average of daily difference between modeled high tide and low tide, where the model output frequency is every 30 min. The modeled tidal range agrees with the historical observation in terms of spatial pattern based on the cross-comparison (Fig. S4a). The model tends to over-estimate the tidal range over the York River mouth while under-estimate the tidal range over the upper end of the Pamunkey and Mattaponi. The largest error of tidal range is 7.98 cm at the station of Northbury, Pamunkey River (Fig. S4a). Due to the uncertainties of cross-comparing historical data and averaged model results, the model performance on simulation the tide is acceptable. Also, harmonic analysis shows that the major constituents are well captured in terms of phases and amplitudes (Fig. S4bc). The model tends to slightly over-estimates the M2 amplitudes by 1.36 cm at the station Sweet Hall and 2.31 cm at the station White House.

Section 5. Evaluations of the realistic case using the conceptual model

To better use the theoretical model for illustrating the change of tidal range over an estuary and the bifurcate responses to SLR with marsh evolution, we applied it to the York-Pamunkey-Mattaponi Estuary. The typical values of the parameters in the theoretical model were computed using the developed 3D numerical model. The results of the base case and the two 1.0 m SLR scenarios for "keep-up" and "give-up" cases were analyzed for illustrating the change of tidal range under SLR.

In the base case, we investigated the changes in tidal range over the Pamunkey River. We selected the start point at the mouth of the Pamunkey River (x = 53.3 km) and the end point at Cousaic marsh (x = 82.2 km) (Fig. 2c), and computed the long-term averages of tidal range, phase velocity, width, and water density at the mouth and the end point (Table S3). Particularly, the phase velocity C was computed as follows. The tide can be decomposed into a series of tidal wave constituents, and in this shallow estuary, the phase velocities for these constituents can be assumed to have the same values. Thus, we only need to compute the phase velocity for the M2 tide component. The phase velocity was computed using wave number (k) and wave angular frequency (ω) as $C = \frac{\omega}{k}$, if we assume the sinusoidal form $\eta = a cos(\omega t - kx)$ for the elevation of the M2 tide constituent (Friedrichs and Aubre, 1994), where a is the amplitude and kx is the phase that can be obtained from the tidal harmonic analysis (Fig. S5). The wave number k at a given location is a function of x, and its value was computed based on the along-channel shifts in the phase for M2 tide constituent (kx) in the numerical model using the equation $\overline{k} = \frac{\Delta(kx)}{\Delta x}$, where the overbar indicates the average over a short distance Δx around the location. Also, $\omega = \frac{2\pi}{T_{M2}}$ and T_{M2} is the M2 tide period and equals 12.4206 hours. After calculating the phase velocity, the nondimensional parameters ε_2 was further calculated using the computed width and phase velocity, and the ε_1 was calculated using Eq. (S5).

In the two 1.0 m SLR scenarios, the values of parameters in Eq. (S5) differ from the base case, which were computed by the numerical model (Table S3). Using the new set of the parameter values, we calculated, for each scenario, the values of $\Delta Shoaling$ and $\Delta Friction$ based on Eq. (S7), which helps to understand how each process contributes to the change in the tidal range under SLR. The trend and magnitude of the changes were compared with numerical results for each scenario.

In addition, the mean elevation, water depth, and width in each scenario were computed for the selected section (x = 53.3 km to 82.2 km) in the Pamunkey River (Table S2). The three parameters were also computed for the York River from the York mouth (x = 0 km) to near the West Point (x = 48.0 km) for comparison.

Table S1. Mean tidal ranges (m) responding to different SLR and marsh accretion ("macc”) conditions for the entire York, Pamunkey, and Mattaponi Rivers, respectively. Note that the scenario “SLR = 1.5 m, marsh keep-up” is the scenario for macc = 1.5 m

Scenarios	**York R.**	**Pamunkey R.**	**Mattaponi R.**
Base	0.781	0.854	0.907
SLR=0.5 m, marsh keep-up	0.801	0.929	0.966
SLR=1 m, marsh keep-up	0.815	0.983	1.009
SLR=1.5 m, marsh keep-up	0.825	1.026	1.039
SLR=0.5 m, marsh give-up	0.791	0.829	0.905
SLR=1 m, marsh give-up	0.782	0.747	0.871
SLR=1.5 m, marsh give-up	0.771	0.734	0.865
SLR=1.5 m, macc=0.25 m	0.786	0.755	0.891
SLR=1.5 m, macc=0.5 m	0.795	0.794	0.914
SLR=1.5 m, macc=1 m	0.820	0.929	0.993
SLR=1.5 m, marsh partial catch-up	0.792	0.872	0.940

Table S2. Mean surface elevation (relative to the mean sea level), mean water depth, and mean width for the Base case in 2010 and two 1.0 m SLR cases for two sections, respectively, in the York River from the mouth (x = 0 km) to near the West Point (x = 48.0 km) and in the selected section in the Pamunkey River from the mouth (x = 53.3 km) to the Cousaic marsh (x = 82.2 km). Note that the mean depth is calculated as the water volume divided by the surface area. SLR of 1.0 m does not increase the mean water depth by 1.0 m when the surface area also increases.

	Base case	**Keep-up case**	**Give-up case**
York River			
Mean elevation (m)	0.140	1.128	1.127
Mean depth (m)	5.204	5.538	5.537
Mean width (m)	2875	3368	3370
Pamunkey River			
Mean elevation (m)	0.182	1.162	1.164
Mean depth (m)	5.872	6.674	3.980
Mean width (m)	540	539	1140

Table S3. Characteristics of tidal range change and the bifurcate responses to SLR of 1.0 m over the selected section in the Pamunkey River with extensive marshes. The start point in the Pamunkey River is set to be at the mouth (*x* = 53.3 km) and the end point is set to be at the Cousaic marsh (*x* = 82.2 km).

Symbols	**Description and units**	**Base case**	**Keep-up case**	**Give-up case**
H_0	Tidal range at start point (m)	0.852	0.954	0.839
C_0	Phase velocity at start point (m s^{-1})	5.511	5.901	5.463
b_0	Width at start point (m)	721	688	1321
ρ_0	Water density at start point (kg m^3)	1005.6	1008.0	1007.0
H	Tidal range at end point (m)	0.828	0.956	0.698
C	Phase velocity at end point (m s^{-1})	8.033	8.713	5.753
b	Width at end point (m)	476	469	1182
ρ	Water density at end point (kg m^3)	1000.7	1001.4	1001.2
ε_1	$\sqrt{1 - F/(E_0 C_0 b_0)}$	0.951	1.003	0.805
ε_2	$\sqrt{Cb/C_0 b_0}$	0.981	1.003	0.971
(H'/H)	The ratio of the new tidal range to the original tidal range at end point	/	1.156	0.843
$(H_0{}'/H_0)$	The ratio of the new tidal range to the original tidal range at start point	/	1.120	0.985
$\Delta Friction$	$\varepsilon_1{}'/\varepsilon_1$	/	1.054	0.847
$\Delta Shoaling$	$\varepsilon_2{}'/\varepsilon_2$	/	1.023	0.990

Fig. S1. The Chesapeake Bay. The blue circles mark the NOAA tide gauges. (b) The York-Pamunkey-Mattaponi Estuary. The red triangles mark the locations with historical tidal range data or observations of elevation along the York River, the Pamunkey River, and the Mattaponi River.

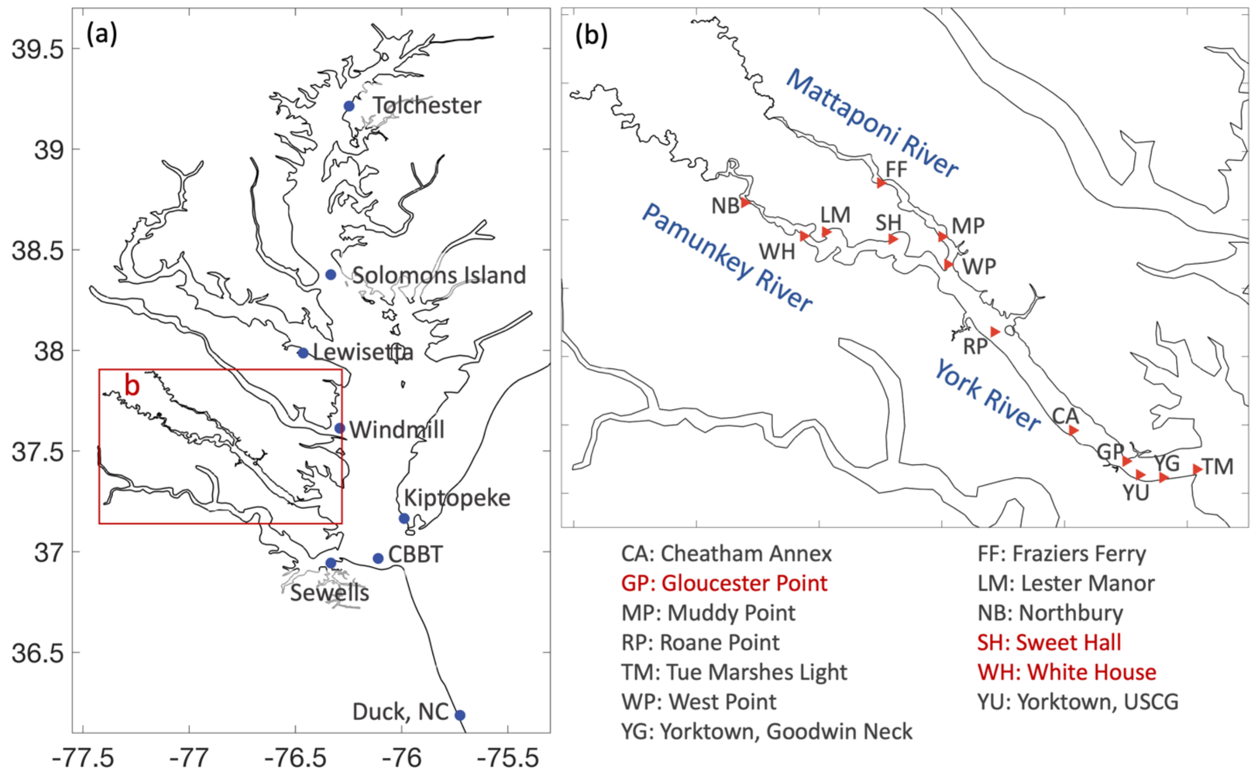

Fig. S2. The SCHISM model domain with zooms on (a) the Sweet Hall marsh, (b) the confluence section of the Pamunkey River and the Mattaponi River, (c) the lower York River, and (d) the lower Chesapeake Bay.

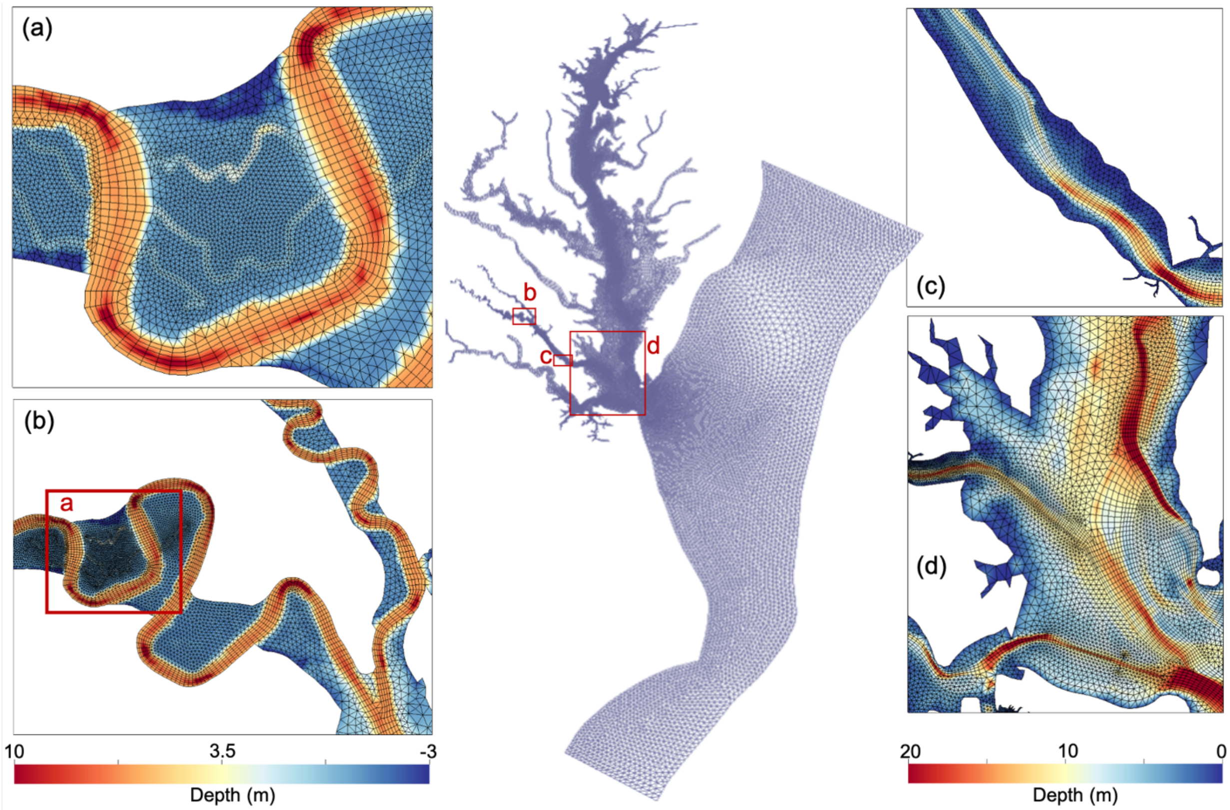

Fig. S3. Tidal harmonics for major constituents in 2010 in NOAA tidal gauges listed in Fig. S1.

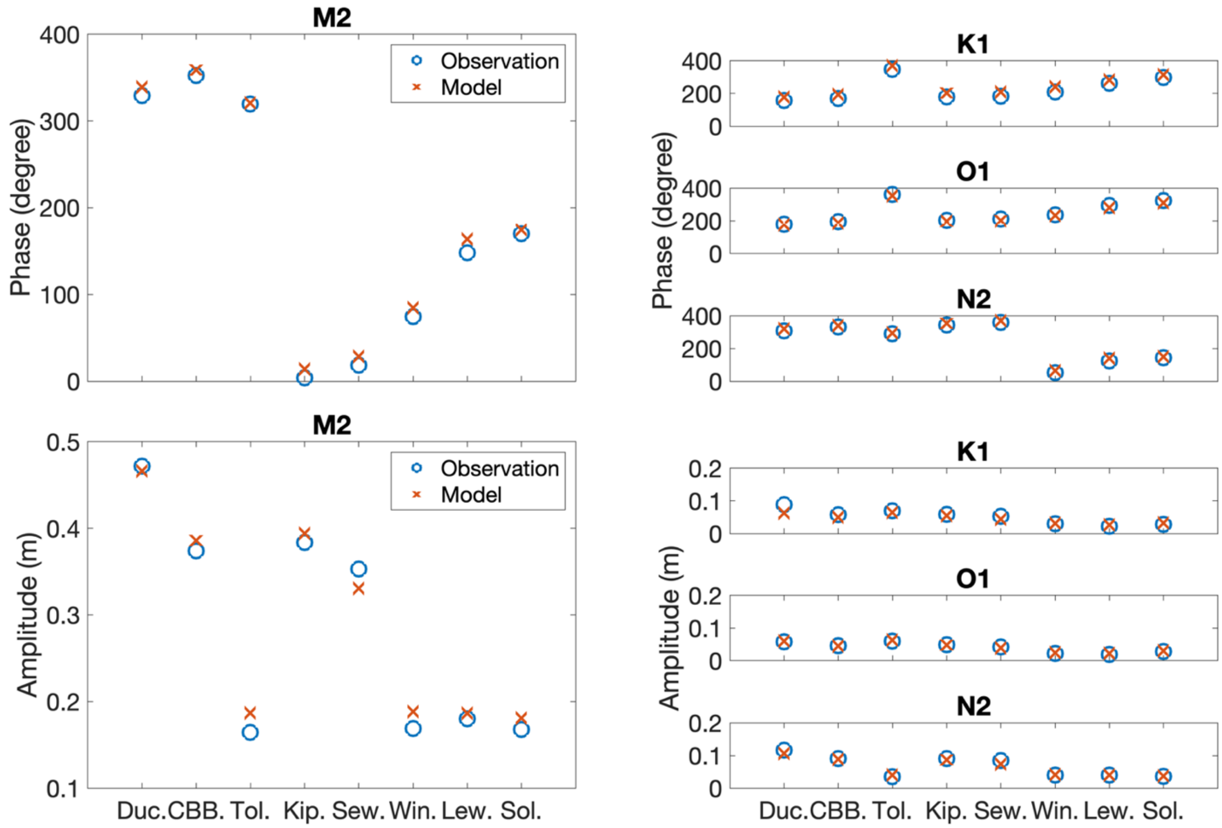

Fig. S4. (a) Comparison between the average of modeled tidal range in 2010 and historical observations in the York-Pamunkey-Mattaponi Estuary. Historical observations are from NOAA tide tables and Virginia Estuarine and Coastal Observing System. (b) and (c): Tidal harmonics for 4 major constituents at two VECOS stations with available observations in 2010 listed in Fig. S1.

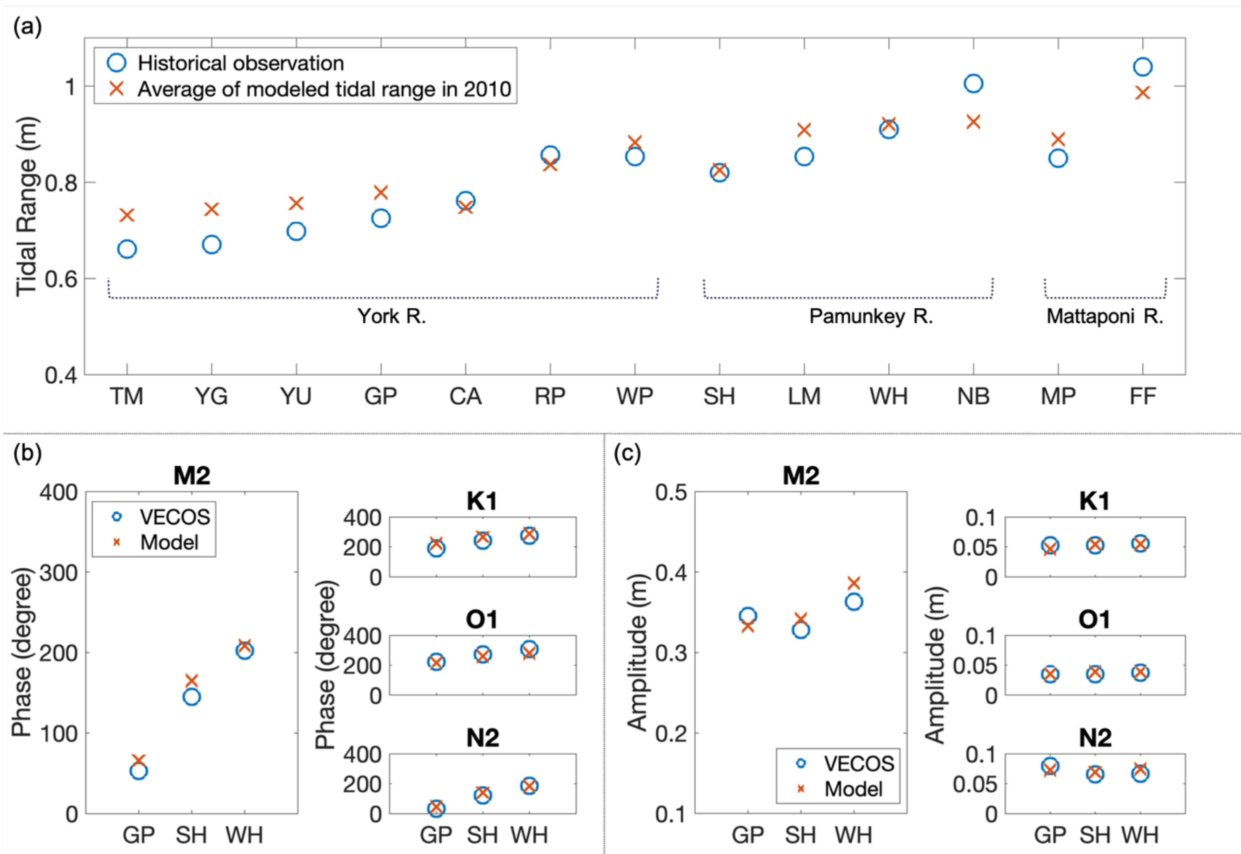

Fig. S5. Tidal phase of the M2 tide component over the distance along the estuary in the Base case, referred to the phase at the mouth.

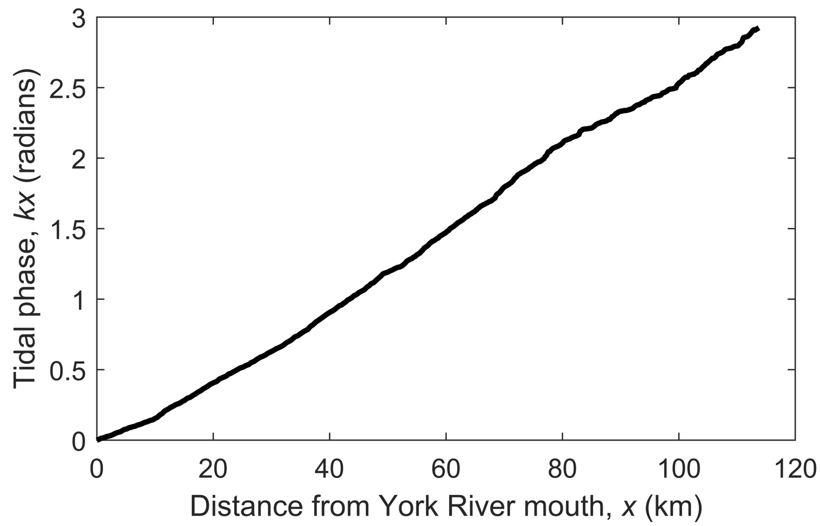

SI references

Brooks, T. J. 1983. Pamunkey River slack water data report: temperature, salinity, dissolved oxygen, 1970-1980. doi: 10.21220/V5XC76

Cai, X., Y. J. Zhang, J. Shen, H. Wang, Z. Wang, Q. Qin, and F. Ye. 2020. A Numerical Study of Hypoxia in Chesapeake Bay Using an Unstructured Grid Model: Validation and Sensitivity to Bathymetry Representation. J. Am. Water Res. Assoc. doi: 10.1111/1752-1688.12887

Friedrichs, C. T., and D. G. Aubrey. 1994. Tidal propagation in strongly convergent channels. J. Geophys. Res.: Oceans, **99**: 3321-3336. doi: 10.1029/93JC03219

Hobbs, C. 2009. York river geology. J. Coast. Res. **10057**: 10-16. doi: 10.2112/1551-5036-57.sp1.10

Jay, D. A. 1991. Green's law revisited: tidal long wave propagation in channels with strong topography. J. Geophys. Res. **96**: 20585–98. doi: 10.1029/91JC01633

Mesinger, F., and others. 2006. North American regional reanalysis. Bull. Amer. Meteor. Soc. **87**: 343-360. doi: 10.1175/BAMS-87-3-343

Nichols, M. M., S. C. Kim, and C. M. Brouwer. 1991. Sediment Characterization of Coastal Lagoons and Bays, Virginian Province. doi: 10.21220/V5BQ60

Prandle, D. 2003. Relationships between tidal dynamics and bathymetry in strongly convergent estuaries. J. Phys. Oceanogr. **33**: 2738–2750. doi: 10.1175/1520-0485(2003)033<2738:RBTDAB>2.0.CO;2

Shenk, G. W., and L. C. Linker. 2013. Development and application of the 2010 Chesapeake Bay watershed total maximum daily load model. J. Am. Water Res. Assoc. **49**: 1042-1056. doi: 10.1111/jawr.12109

Toffolon. M., and H. G. Savenije. 2011. Revisiting linearized one-dimensional tidal propagation. J. Geophys. Res. **116**: C07007. doi: 10.1029/2010JC006616

van Rijn, L.C. 2011. Analytical and numerical analysis of tides and salinities in estuaries; part I: tidal wave propagation in convergent estuaries. Ocean Dyn. **61**: 1719-1741. doi: 10.1007/s10236-011-0453-0

Ye, F., and others. 2018. A 3D unstructured-grid model for Chesapeake Bay: Importance of bathymetry. Ocean Model. **127**:16-39. doi: 10.1016/j.ocemod.2018.05.002

Zhang, Y. J., N. Gerdts, E. Ateljevich, and K. Nam. 2020. Simulating vegetation effects on flows in 3D using an unstructured grid model: model development and validation. Ocean Dyn. **70**: 213-230. doi: 10.1007/s10236-019-01333-8

Zhang, Y. J., F. Ye, E. V. Stanev, and S. Grashorn. 2016. Seamless cross-scale modeling with SCHISM. Ocean Model. **102**: 64-81. doi: 10.1016/j.ocemod.2016.05.002